This document was prepared in conjunction with work accomplished under Contract No. DE-AC09-96SR18500 with the U. S. Department of Energy.

DISCLAIMER

EVALUATION OF MINIATURIZED INFRARED SENSORS FOR PROCESS CONTROL OF THE PALLADIUM MEMBRANE REACTOR (U)

R.J. Lascola
D.W. Howard

July, 2005

Analytical Development Section
Savannah River National Laboratory
Aiken, SC 29808

SRNL
SAVANNAH RIVER NATIONAL LABORATORY

DISCLAIMER

EVALUATION OF MINIATURIZED INFRARED SENSORS FOR PROCESS CONTROL OF THE PALLADIUM MEMBRANE REACTOR (U)

R.J. Lascola
D.W. Howard

July, 2005

Analytical Development Section
Savannah River National Laboratory
Aiken, SC 29808

SRNL
SAVANNAH RIVER NATIONAL LABORATORY
TM

REVIEWS AND APPROVALS

AUTHOR(S):

_____   August 18, 2005
Robert J. Lascola, Analytical Development Section / MTD / SRNL   Date

_____   08/18/2005
David W. Howard, Hydrogen Technology Section / SMTD / SRNL   Date

TECHNICAL REVIEWERS:

_____   August 18, 2005
Laura L. Tovo, Analytical Development Section / MTD / SRNL   Date

APPROVERS

_____   8/22/05
S.R. Salaymeh, Manager, Sensors & Analyzer Technology Group / ADS   Date

DERIVATIVE CLASSIFICATION:

_____   August 18, 2005
Laura L. Tovo, Analytical Development Section / MTD / SRNL   Date

EXECUTIVE SUMMARY

We have tested the suitability of a miniaturized infrared sensor for measurements of CO and H_2O in the inlet stream to the Palladium Membrane Reactor (PMR). We demonstrated that both analytes can be measured with absolute accuracies of 2-4% at the process inlet conditions of 120-140 ^{o}C and approximately 1 atm of each gas. This accuracy must be improved to 1-1.5% for effective PMR process control. The use of a reference detector and independent temperature and pressure measurements to correct the raw signals will improve the accuracy to a level that will approach, if not meet, this goal. With appropriate bandpass filters, the infrared sensors may be used for other gas analysis applications.

TABLE OF CONTENTS

LIST OF FIGURES

LIST OF TABLES

LIST OF ACRONYMS

au	Absorbance units
GC	Gas chromatography
IR	Infrared (absorption spectroscopy)
LANL	Los Alamos National Laboratory
MS	Mass spectroscopy
PMR	Palladium Membrane Reactor
SRNL	Savannah River National Laboratory

1.0 INTRODUCTION AND BACKGROUND

The Palladium Membrane Reactor (PMR) is designed to recover hydrogen isotopes from water present as an impurity in tritium processing activities.[1,2,3] In the PMR, water and carbon monoxide (CO) are catalytically reacted to form carbon dioxide (CO_2) and hydrogen at elevated temperatures and pressures (up to 425 ^{o}C and 2-3 atmospheres, respectively). The hydrogen is recovered by diffusion through a palladium (Pd) membrane (driven by the partial pressure difference between the process pressure on one side and vacuum on the other side), which is selectively permeable to hydrogen. Most hydrogen will be present as protium. Only trace amounts of deuterium and tritium are expected.

The efficiency of the PMR reaction is governed by the CO/water concentration ratio. A slight excess of CO improves the kinetics of the reaction and promotes complete conversion of the water to elemental hydrogen; however, too much CO leads to fouling of the catalyst and/or Pd membrane with elemental carbon (soot), degrading the performance of the PMR. The recent failure of several Pd membrane tubes at Savannah River National Laboratory (SRNL) may be attributable in part to an excess of carbon, which may have been incorporated into the metallic structure, making it more susceptible to deformation and leaking.

The desired CO/water ratio is within a narrow range, 1.05-1.1. This suggests that the water and CO pressures must each be measured with absolute accuracies of 1-1.5% to obtain effective process control.[*] The consequences of operation outside this band for an extended period of time highlight the need for accurate quantitation and control of the feed gases. The historical approach used to maintain the proper ratio is to measure and control the mass flow rates of each species individually before mixing them. Development work at Los Alamos National Laboratory (LANL) and SRNL has shown this approach to be not entirely satisfactory, as the mass flow measurement devices have not been sufficiently accurate to prevent process upsets. Therefore, flow control based on a more precise and reliable measurement technique is desirable.

Several techniques which have been widely applied to the general problem of process gas analysis include gas chromatography (GC), mass spectroscopy (MS), and infrared spectroscopy (IR).[4] However, GC and MS are not particularly suitable to PMR feed gas analysis. The feed gas is maintained at temperatures near 140 ^{o}C to keep water vaporized at high pressures. Process measurements with both GC and MS require capillaries to transport the sample to the instrument. Thus, extensive heat tracing is required to keep water from condensing in the lines, and the finite transport time of the gas makes these methods less responsive.   Also, procurement and maintenance costs for these instruments are substantial.

Infrared spectroscopy is more amenable to the analysis problem, as it is readily introduced into the process environment and the target analytes are detectable at the process conditions. There are several IR techniques which could be considered. Fourier transform absorbance [5] and

---

[*] For example, a 1.25% uncertainty for a target CO pressure of 1.075 atm yields a range of 1.062 – 1.088 atm. To maintain the CO/water ratio within the desired limits, the H_2O pressure must be between 0.989-1.011 atm. This range represents a 1.1% spread from the target pressure of 1.0 atm.

emission [6] spectroscopy, tunable diode laser spectroscopy [7], and cavity ring-down (time-based) spectroscopy [8] have all been successfully demonstrated for trace gases, and are commercially available. However, the capabilities of these methods are all far greater than what is required for the application. Instead, we have concentrated on finding a simple instrument that can be economically installed at several locations and is easy to operate.

Infrared plug sensors [9] meet this description. The plugs are small, rugged, and self-contained[*]. They can be placed directly in the process stream and do not require fiber optics. They can be obtained in a variety of sampling configurations. Liquids and solids can be measured with attenuated total reflection on a single plug, while gases are analyzed by absorbance across the pipe diameter with separate source and detector plugs. Since the water and CO are the only stream constituents, and have absorptions that are spectrally distinct, an IR spectrometer is not required for the measurement. Instead, one may simply use two or three detectors whose wavelength responses are defined by bandpass filters.

This report describes characterization work done on one type of sensor, the Infraran model produced by Wilks Enterprises (Norwalk, CT). We studied the temperature and pressure dependence of the sensor response, potential interference effects occurring from different gas mixtures, short- and long-term accuracy and precision, the effect of different signal averaging options, and other environmental effects.

2.0 EXPERIMENTAL

2.1 Sensors

Figure 1 shows the gas cell and the sensor housing. The light source (labeled "A") is a pulsed diamond thin-film element, with an output approximated by a black body temperature of 800-850 ^{o}C. There are two pyroelectric detectors mounted in a T08 can housing on the opposite side of the cell from the light source (labeled "B"). Glued in front of each detector is an infrared bandpass filter corresponding to either CO or H_2O vibrational absorptions (near 4.7 and 2.7 μm, respectively). Figure 2 shows the blackbody emission and filter transmission spectra for these elements. No reference detector was provided. The source and detector interface the gas cell through cubic zirconia windows (2 mm thickness, 12.5 mm diameter) which are sealed with epoxy. The windows define a 3 mm absorption path length.

---

[*] Typically the plugs are 2" diameter. They have been tested to 150 psi and 100 ^{o}C. The light source and detector are mounted on the plug. Processing electronics can be on the plug or in a separate box.
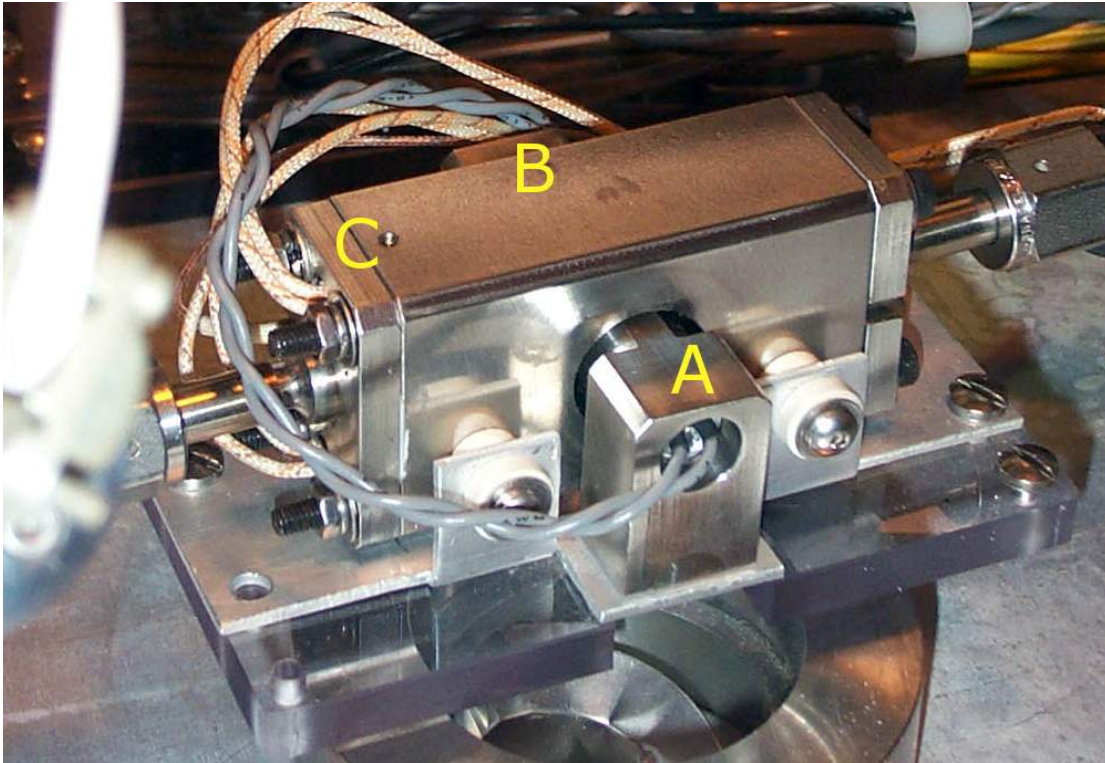
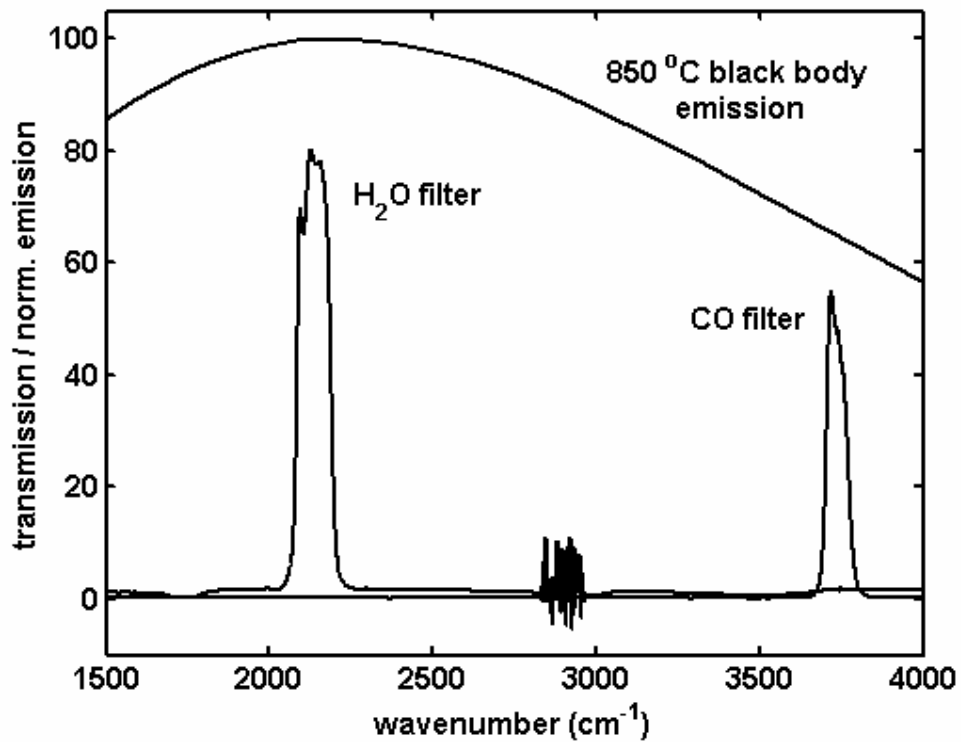**Figure 1. Photograph of infrared cell.**

Figure 2. Spectral profiles of IR filters and source.

The sample cell is constructed from stainless steel and is approximately 10 cm long and 2.5 cm wide. The internal cell volume has a rectangular cross-section 3 mm wide and 10 mm high. End caps with ¼" female VCR fittings are attached to the cell with four pass-through bolts; seals are maintained with rubber gaskets. There are three holes in the sample cell body parallel to the internal cell. Two holes house cartridge heaters (labeled "C" in Figure 1), and the third contains a thermocouple. These elements are connected to a temperature regulator.

Other supporting electronics include a control module that provides power to the source and detectors and monitors the detector output, and a processing unit that maintains the calibration and displays results. Output can also be logged onto a computer through a standard serial cable connection.

2.2 Gas Handling

The sample cell was spliced into a gas handling manifold which had previously been constructed for testing a PMR prototype. All lines were heat-traced by wrapping them in heating tape, foam insulation, and aluminum foil, and installing thermocouples to monitor the temperature. Minimum temperatures of 120 ^{o}C were set in order to maintain water in the vapor phase at elevated pressures. Pressure was measured at several points in the manifold, including adjacent to the gas cell. CO was introduced from a standard gas cylinder (Scott). Steam was taken from a facility steam line. The entire gas system, including the sensor but not the display electronics, was contained in a large walk-in hood. Several CO and CO_2 atmospheric sensors were employed to monitor leaks.

Sensor readings were obtained with gas pressures ranging from 14.5 - 40 psi. Readings were made on a static system. The pressure was varied by sequentially bleeding in or releasing a small amount of gas and allowing the system to equilibrate for 30-60 seconds. This time period was determined both by the signal averaging of the instrument (typically 30 seconds) and by gas transport issues associated with the narrow dimensions of the cell.

In the course of the work, two problems developed which precluded us from making all the desired measurements. First, it proved to be very difficult to maintain heat tracing so that water vapor did not condense somewhere in the line. Thus, water measurements were made on a dynamic system, where the instantaneously measured absorbances were compared with instantaneous pressures. Thus, the data obtained for those experiments did not have the same advantage of signal averaging as the CO data. Second, we intended to create CO/H_2O mixtures inside the sample cell by introducing a known pressure of one gas into the cell and then applying a greater pressure of the second gas. In testing this arrangement with CO and argon, we found that we could not remove residual amounts of the first gas added from lines leading to the cell. Thus, when the second gas was added, it swept in a certain amount of the first gas, and thus partial pressure of the first gas was not left constant. Due to time and equipment constraints, we were not able to install a vacuum pump to clear out those lines. We also could not heat trace a reservoir which would have been a more suitable gas mixing chamber.

2.3 Calculations

Sensor response calculations were performed with Matlab, version 6.1 (Mathworks, Natick, MA). IR absorption spectra of CO and H_2O were calculated from the 2000 HITRAN database using HITRAN-PC (ONTAR, N. Andover, MA). Bandpass filter spectra were provided by the vendor. Light source output was calculated assuming a 850°C black body source with a Web-based applet from Lawrence Berkeley Laboratory [10].

3.0 RESULTS AND DISCUSSION

3.1 Experimental Results

The sensor testing concentrated on those aspects associated with use in a process environment. Process temperature and pressure variations, external influences, and chemical changes must all be accommodated. A sensor could be insensitive to these factors, or its variations must be corrected by incorporating other measurements (typically pressure and temperature). Stability of the sensor, independent of process changes, must also be considered. A thorough understanding of these factors is required to assess both the viability of the sensor for the application and the resources needed to install and operate the sensor.

3.1.1 Sensor Stability

The Infraran sensors are designed to be operated at temperatures below 80-100 ^{o}C. The limiting factor is expected to be the temperatures at which the on-board electronics can reliably operate. Since the gas temperature in the PMR system must be 120-140 ^{o}C to keep water in the vapor phase and improve the system efficiency, some accommodation must be made to protect the sensors while making the measurement. For the current system, this is done by using ceramic standoffs to maintain physical separation of the sensor mounting brackets and the gas cell. However, the separation between the sensor and the cell is only a few millimeters, and thus the sensors are likely to be near the upper end of their recommended operating temperature.

We therefore conducted a stability test to show that the sensors would operate effectively under these conditions. The cell was heated to 120 ^{o}C, pressurized with Ar (~39 psi), and sealed. The sensors were zeroed and the system was maintained at these conditions for over 30 hours. The measured absorbances (using a 30-second rolling average) for both CO and H_2O channels are shown in Figure 3. With the exception of a relatively large spike near 1000 minutes, as seen in Figure 3a, and a similar feature at the beginning of the study, the response of both sensors is stable (standard deviations of 0.0032 and 0.0046 absorbance units (au), respectively).
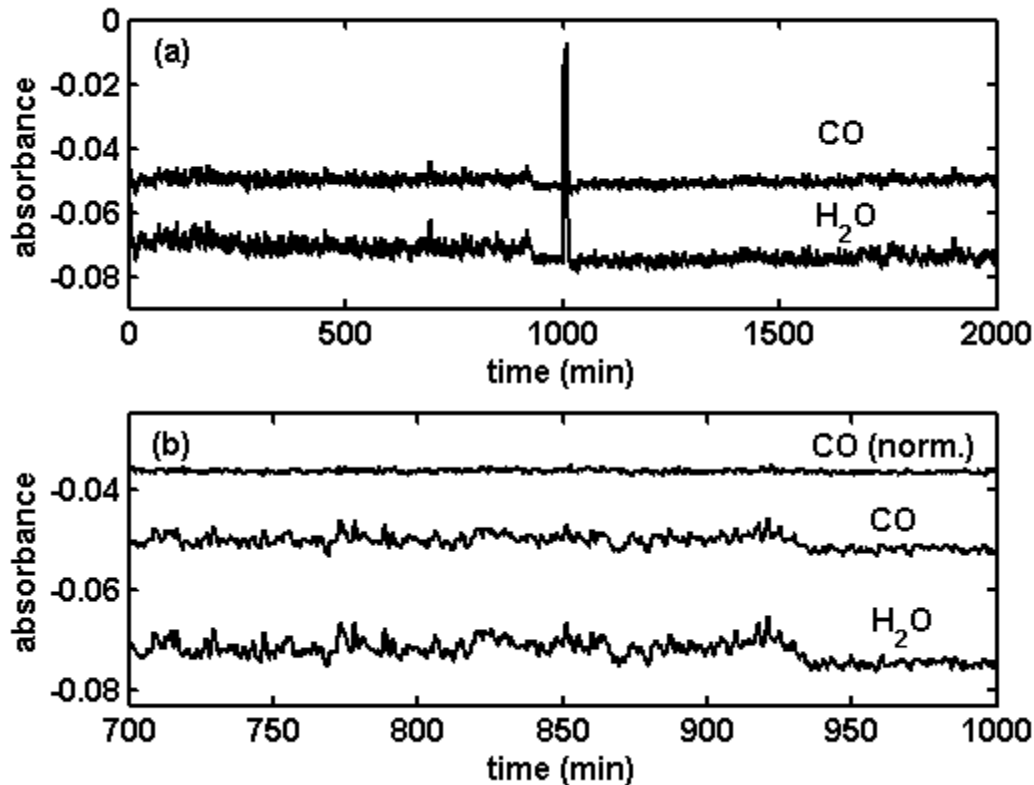
Figure 3. Stability and noise characteristics of detectors.

Several features of the figure merit further discussion. The sensors were located inside a walk-in vent room. After the sensors were zeroed, the vent room doors were closed, and both sensors recorded a 0.05-0.07 au offset that was maintained as long as the doors were closed. The sharp spikes back toward zero occurred when the doors were opened to look at the sensors. Further investigation revealed that when the doors were closed, there was a strong air flow through an opening at the top of the room directly onto the sensors, presumably cooling them. This behavior suggests that if the Infraran were to be used in a hot process environment, care would have to be taken to have the environmental conditions remain as consistent as possible. Sensor drift on this scale is much greater than the intrinsic sensor noise, and is significant on the scale of absorbance changes caused by CO and H_2O with this gas cell.

An expanded view of the sensor response (Figure 3b) shows that the CO and H_2O noise is highly correlated ($\rho = 0.79$), supporting the suggestion that environmental variations in this test are greater than intrinsic sensor variations. The latter can be estimated by treating the H_2O channels a reference and dividing it into the CO channel response to normalize the latter. After multiplying by the H_2O channel average (about 0.07 au), one obtains the top trace in Figure 3b, which has less variation than the individual curves. The standard deviation of the normalized set is 0.00091 au, which is 3.5 times better than the raw signal. The improved performance strongly suggests that a reference channel should be used in future configurations.

6

3.1.2 CO Sensor

Absorbance values as a function of system pressure were obtained for 100% CO at temperatures ranging from 23 - 140 $^{\circ}$C. The absorbance increased monotonically with pressure increase, and the results are reproducible across several pressure cycles. Typical data (120 $^{\circ}$C) showing the dependence of pressure (measured in absolute psi) on absorbance, along with a best fit line, are shown in Figure 4. Although the absorbance was the dependent variable during data collection, it is shown as the independent variable to be more representative of how the sensor would be used in practice.
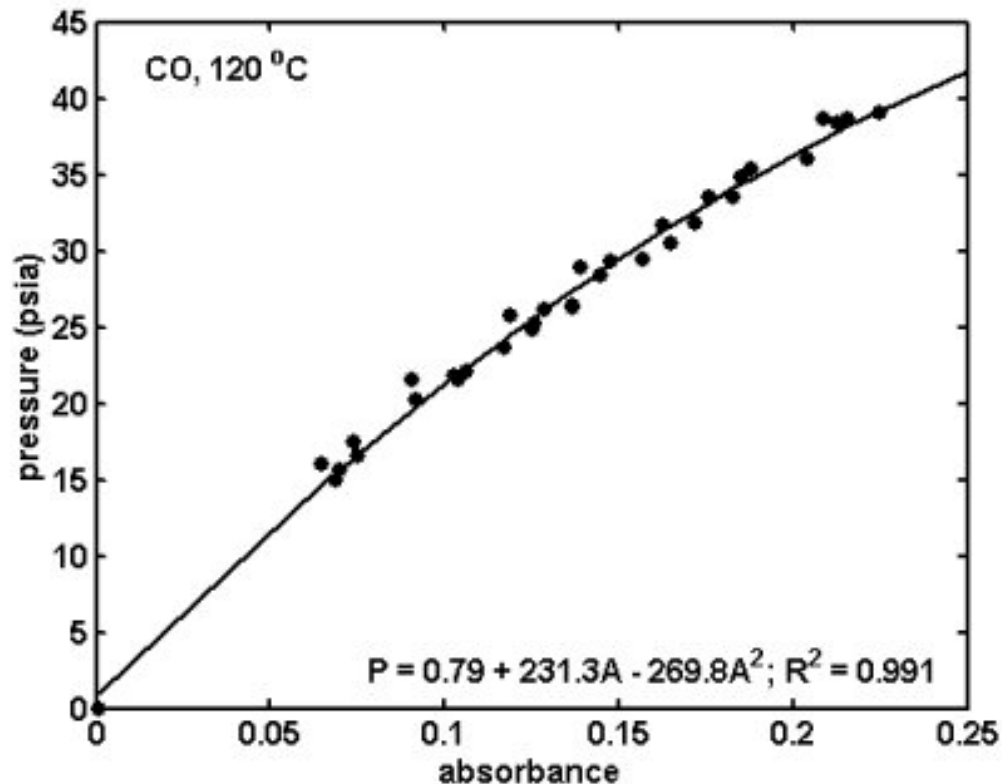
Figure 4. Relationship between pressure and absorbance for CO.

Table 1 shows the quadratic fit parameters for each temperature (P(psia) = $a_0 + a_1A + a_2A^2$). Several points are apparent. The intercepts (a_0) are zero or nearly zero for all temperatures. The linear coefficients (a_1) generally increase with temperature. This may be expected if the increasing temperatures result in the population of higher rotational levels, which would lead to more absorption lines appearing within the filter bandpass (at the expense of lines outside the bandpass). Thermal expansion of the cell may also account for a small portion of the increase. The quadratic term (a_2) is statistically significant at all temperatures, which represents a deviation from the linear behavior predicted from Beer's Law.[*] However, nonlinearity may be

---

[*] A = εbc, where ε is the absorptivity of the molecular transition, b is the measurement pathlength, and c is the concentration.

expected under certain conditions which are met in these measurements. This topic will be further examined during the discussion of sensor response calculations, below.

Table 1. Temperature dependence of CO absorbance.

T (^{o}C)	a_0 (1ς)	a_1 (1ς)	a_2 (1ς)	R^2	Std err (%)
23	0.88 (0.76)	129 (7)	-49 (17)	0.9976	1.6
50	0.03 (0.55)	160 (6)	-105 (18)	0.9894	2.6
85	2.3 (0.7)	188 (10)	-154 (34)	0.979	3.3
120	0.8 (0.7)	231 (11)	-270 (42)	0.991	3.3
140	4.7 (0.3)	220 (5)	-181 (22)	0.9982	1.4

Note also that each fit replicates the measurements within 2-3%. This accuracy is consistent with the control requirements described above. However, these tests were conducted under controlled conditions and were of a relatively short duration. Greater uncertainties, and the need for compensatory measurements, would be expected in less controlled conditions.

3.1.3 H_2O Sensor

For reasons described in the experimental section, it was not possible to get time averaged absorbance data for a fixed water vapor pressure in the cell. Consequently, the uncertainties associated with this analysis are greater than for the CO analysis. There is no reason otherwise that the analysis of water vapor should be any less accurate than for CO; therefore, the results reported here should not be considered a true measure of the potential system performance. Data was only acquired at 140 ^{o}C, so no temperature dependence of the coefficients was obtained. The 140 ^{o}C data is presented in Figure 5. The sensor response to water is similar to the CO response, particularly with the statistically significant negative quadratic dependence on absorbance.

3.1.4 Analyte Independence

Because both the water and CO measurements are univariate (relying on the signal of a single detector), accurate measurement of each requires that the measurements be independent. Independence must not only be intrinsic, e.g. there are no overlapping absorption peaks, but also extrinsic, e.g. water and CO do not interact so as to appreciably change the absorption of either.

Intrinsic independence is expected based on calculations using the HITRAN atmospheric database; there are no CO absorptions predicted in the 3680-3800 cm^{-1} range of the H_2O filter, nor are there H_2O absorptions in the 2060-2210 cm^{-1} range of the CO filter. Measurements of pure CO and pure H_2O vapor confirm this result. The correlation coefficient (ρ) for the CO sensor in the presence of water is 0.12. The correlation coefficient for H_2O in the presence of CO is somewhat larger, 0.29, but this value may reflect environmental effects, as discussed above. These results confirm that the detectors are intrinsically independent.
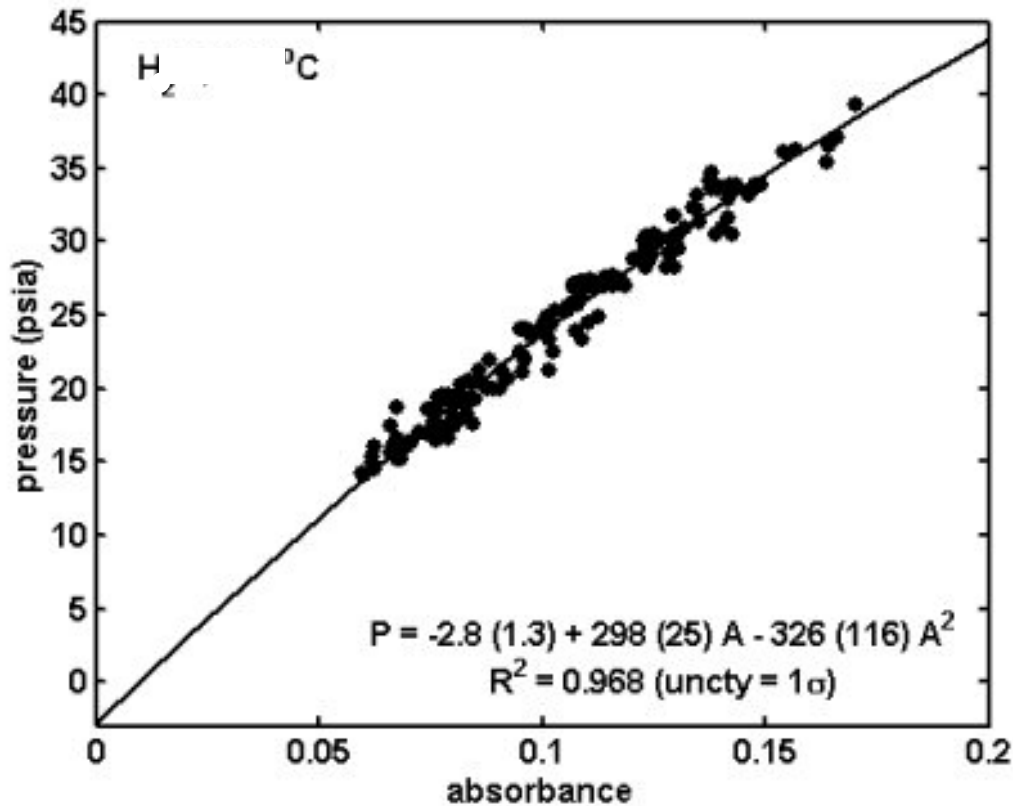
Figure 5. Relationship between pressure and absorbance for H₂O.

Extrinsic interactions may be considerable given the strong hydrogen-bonding potential of H_2O and CO. The effect of these interactions on gas number density, which in turn affects absorption, can be estimated from the van der Waals gas equation [11]:

$$\left(P + \frac{a}{v^2}\right)(v - b) = RT$$

$$v = \frac{V}{n}$$

Here, P, V, and T are the system pressure, volume, and temperature, R is the ideal gas constant, n is the total moles of gas, and a and b are molecule-specific interaction constants. The molar gas density is represented by v^{-1}. For a mixture, the effective interaction constants can be determined from the constants for the components:

$$a_{eff} = \sum_i \sum_i f_i f_i (a_i a_i)^{\frac{1}{2}}$$

$$b_{eff} = \sum_i \sum_j f_i f_j (b_i b_j)^{\frac{1}{2}}$$

9

where each summation is over all components, and f_i is the molar fraction of the ith component.

The effect of water on CO number density, and *vice versa*, can be seen in Figure 6. Here, the partial pressure of the labeled component is fixed at 14.7 psia (1 atm), while the partial pressure of the other component varies from 7.35 to 22.35 psia. The effect is plotted as a deviation from the ideal gas law. This calculation also takes into account self-interactions (e.g. CO-CO or H_2O-H_2O). It may be seen that near the typical PMR operating conditions of 2 atm total pressure, the number density correction for each gas is approximately 0.5%. The correction changes by a few tenths of a percent with expected temperature and pressure variations within the PMR process.
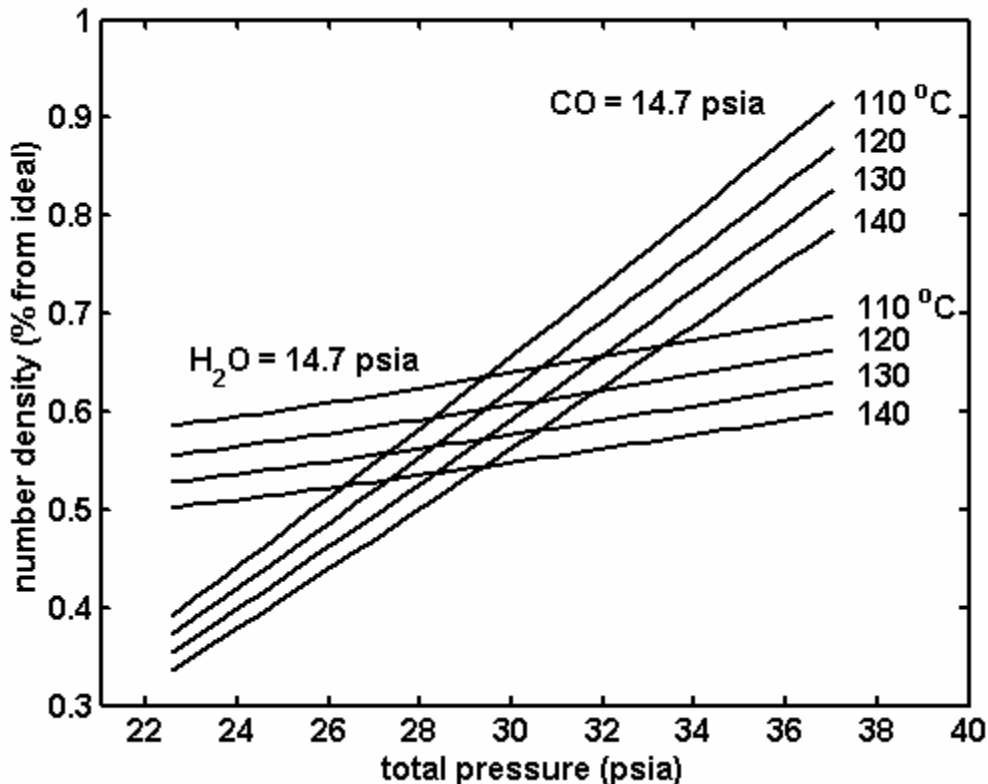
Figure 6. Pressure-dependent deviation from ideal gas law.

This change is significant compared to the desired 1-1.5% uncertainty of the measurement. However, a correction based on a temperature measurement can be made readily. As both intrinsic and extrinsic interactions are negligible or correctible, we can conclude that the water and CO signals are adequately independent.

3.1.5 Signal Averaging
The sensor manufacturer supplied the control system with a fixed rolling average of 30 seconds applied to the displayed gas concentrations. We wished to determine if a shorter time constant would provide adequate noise reduction while allowing for a faster system response. The data stream includes instantaneous intensity readings, which can be converted to absorbances. A

section of this data for a CO cycling experiment is shown in Figure 7. In addition to the raw data, data averaged over 7.5, 15, and 30 seconds is shown. Averaged data is offset for clarity.
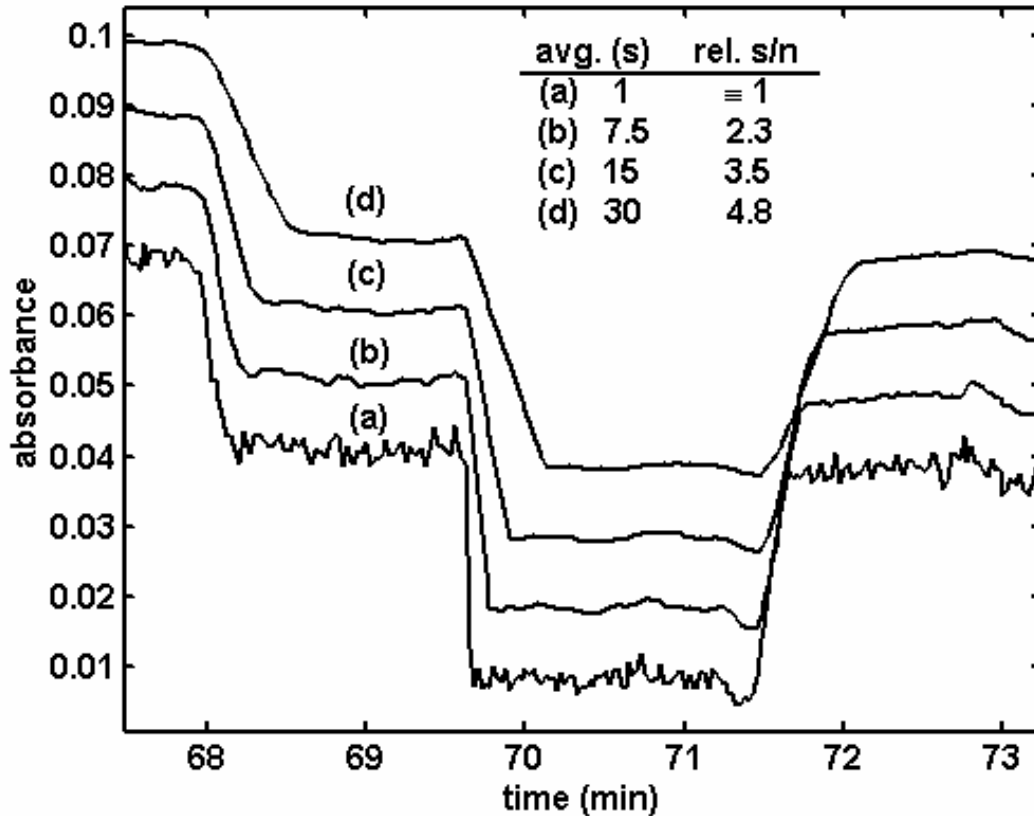
Figure 7. Effect of signal averaging.

Noise reduction, as measured by the standard deviation of the signal with constant CO, improves at a rate slightly less than the square root of the relative time constant. The effect of the time constant on the response to a (near-)instantaneous change in gas concentration can also be seen.

The fit results of Table 1 suggest that the longer signal averaging should be maintained. However, as environmental variations have been shown to play an important role in sensor response, the use of a dedicated reference detector may allow for a shorter averaging time.

3.2 Calculation Results

We supplemented the experimental measurements with calculations simulating sensor response under a variety of conditions. In some cases, this approach was required because we could not successfully prepare gas mixtures with water vapor. In other cases, the sensor/flow cell configuration (e.g. pathlength) could not be changed. The calculations expand our understanding of sensor properties. They can also serve as a template for predicting the viability of the sensors for applications with different operating conditions and/or analytes.

3.2.1 Methodology

The signal generated by each detector can be calculated by convolving the effects of each optical element on the spectrum of the light propagated through the system. The four primary elements are the source, sample, filters, and detector:

$$S(\omega) = I_{lamp}(\omega) \times T_{sample}(\omega) \times T_{filter}(\omega) \times Q_{detector}(\omega),$$

where S represents detector signal, I light intensity, T transmission, and Q quantum efficiency, all of which are dependent on the light frequency, ω.

Several assumptions are made with the calculations. Detector efficiency is assumed constant over the frequency range defined by an individual filter ($Q_{detector} = 1$). Likewise, any reflections at the interfaces in the optical path are assumed not to have a frequency dependence.

Calculations are made for a discrete array of frequencies defined by the highest-resolution data set, which in this case is T_{sample}. The other factors, I_{lamp} and T_{filter}, are interpolated to the higher resolution with a spline fit. Calculations were made with different resolutions for T_{sample}, and consistent results were obtained for resolutions smaller than or equal to 0.01 cm^{-1}. Because the finer resolutions require a larger data set, the maximum spacing was used for subsequent calculations.

S is summed over all frequencies to determine a total signal. Absorbance is calculated from the ratio of the signals for a "zero" gas and the analyte:

$$A = -\log_{10}(S_{analyte} / S_{zero}).$$

T_{sample} is calculated using the HITRAN database [12], which includes linewidth, intensity, pressure coefficients, and other parameters for all observed infrared, visible, and ultraviolet spectral lines for a number of atmospherically important small molecules. The calculation of gas transmission profiles requires the control of a large number of parameters. All gas concentrations apart from H_2O and CO were set to zero. Temperatures and partial and total pressures were specified. A horizontal beam path was selected to remove any altitude effects on the calculation. The smallest available pathlength (1 cm) was chosen. As this value is larger than the gas cell pathlength (0.3 cm), a correction to the results was made (see below).

3.2.2 Comparison to Experiment

The ability of a calculation to replicate experimental results gives a measure of confidence for subsequent calculations. There are two experiments in this study for which a comparison can be made – measurement of CO absorbances at a given temperature, and the replication of temperature-dependent absorption trends for CO.

The comparisons require a correction of the long pathlength used in the calculations. Beer's Law, which describes a linear relationship between pathlength and absorbance, does not apply when absorbances are saturated (e.g. all of the light at a certain frequency is absorbed by the

sample). In these cases, the absorbance will be less than predicted from a linear extrapolation from shorter pathlengths. This is seen in Figure 8, which shows the calculated absorbance for different pathlengths and CO pressures. There is a readily apparent quadratic component to the dependence that is more pronounced for higher pressures. This feature is consistent with more saturated transitions within the filter transmission envelope at the higher pressures. It is also interesting to note the onset of nonlinearities at relatively low absorbances. This occurs because the absorbance is an integrated quantity that includes both saturated transitions and regions with no absorbance. Therefore, the average absorbance for the region is less than what is normally observed when a transition becomes saturated.
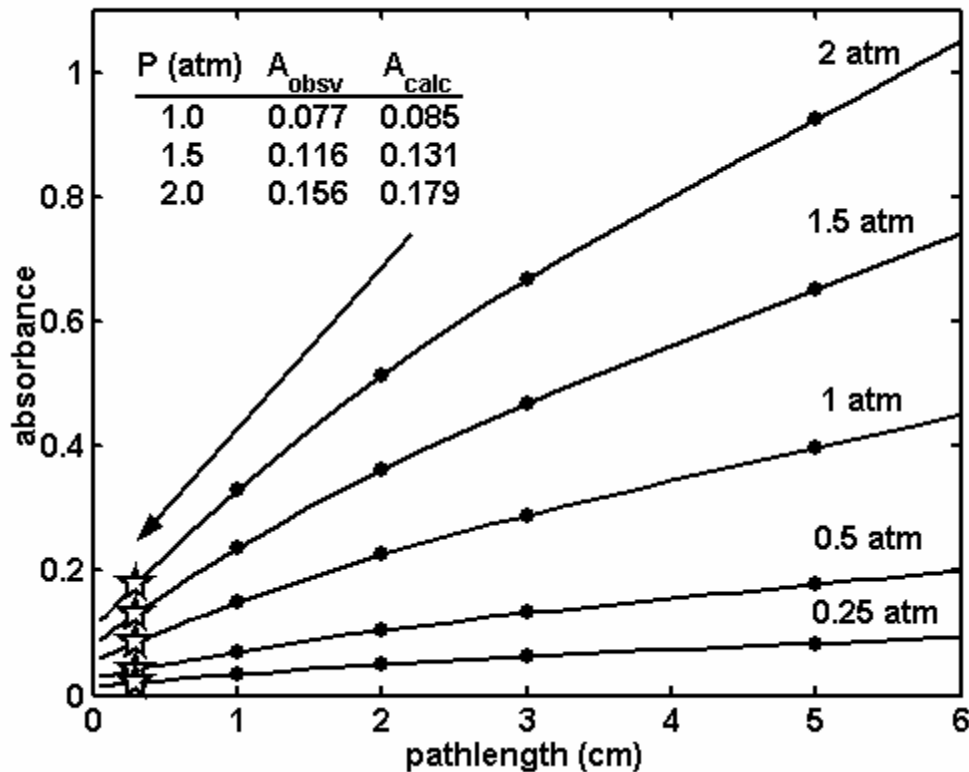
Figure 8. Relationship of pathlength and absorbance.

There are hundreds of narrow absorbance lineshapes within the filter transmission envelope. The number of saturated transitions increases with increasing pathlength, and is non-zero at the shortest available pathlength for the calculation. It is reasonable to assume that at shorter pathlengths, the number of saturated transitions will decrease proportionally. Thus, we can estimate absorbances for the cell pathlength by extrapolating a spline fit to the calculated absorbances. The predicted absorbances for the cell are shown by the stars in Figure 8, and the values are compared to experimental results in the inset. There is good agreement between the two values, considering the inherent assumptions. The agreement indicates that the calculations are representative of experimental results.

A similar level of agreement between experiment and calculation is seen for the temperature dependence of absorbance, as shown in Table 2. Here, the CO or H_2O pressure was fixed at 14.7 psia (1 atm). Absorbances are calculated for 1 cm and corrected to 0.3 cm by dividing by 1.75, the ratio determined from Figure 8.

Table 2. Temperature dependence of CO and H_2O absorbance.

Temp (K)	298	323	358	393	413
A_{CO} (obsv.)	0.115	0.100	0.072	0.071	0.063
A_{CO} (calc.)	0.103	0.098	0.093	0.088	0.085
A_{H2O} (calc.)	0.063	0.062	0.061	0.060	0.059
A_{CO} / A_{H2O}	1.63	1.58	1.52	1.46	1.43

The observed and calculated CO absorbances both decrease as temperature increases (the temperature dependence is less marked for the calculation). One contributing factor is the decrease in CO number density caused by fixing both pressure and volume while changing the temperature. Another is a temperature-induced population shift to higher rotational ground states that favors transitions that are outside the filter envelope.

The ability of the calculations to replicate CO absorption measurements and temperature-dependent trends gives a measure of confidence that similar calculations will give good results.

3.2.3 Temperature Effects on Water Absorbances

Table 2 also shows the calculated effect of temperature on water measurements. As with CO, there is a decrease in the absorbance, though the decrease is much smaller (6% versus 17% between 298 and 413K). This is due to the rotational energy level distribution for water. For this symmetric top molecule, transitions from different rotational ground states are interspersed instead of being in a regular progression, as is the case for a diatomic molecule. Thus, population transfer to higher energy states does not change the line overlap with the filter envelope as much as occurs for a diatomic.

Note that the ratio of the CO and H_2O absorbances changes by 2% in the expected PMR process range of 120-140 ^{o}C. This deviation can be readily corrected if the temperature is independently measured.

3.2.4 Pressure Broadening

Molecular absorption profiles are sensitive to pressure broadening effects. [13] Specifically, linewidths will increase due to a decrease in excited state lifetimes and an increase in energy level perturbations. This effect is manifested through an intrinsic change in the analyte (the absorptivity) and so differs from the extrinsic changes described above. Note that for a strongly saturated transition, the peak will remain saturated despite the transfer of absorption strength to the wings of the transition. Since there are many such transitions within the filter envelope, pressure broadening is expected to increase the overall absorbance at a given analyte partial pressure.

Pressure broadening effects for CO and H_2O were calculated for expected PMR process conditions. The target gas was assumed to have a partial pressure of 14.7 psia (1 atm), with air providing the balance of the total pressure.[*] Total pressure ranged from 26.5 to 32.3 psia (1.8 – 2.2 atm). The temperature was fixed at 140 ^{o}C. The pathlength was 0.01 m. Results of the calculation are shown in Table 3.

Table 3. Pressure broadening of CO, H_2O absorbance.

P_{total} (atm)	1.8	1.9	2.0	2.1	2.2
$A_{CO\ (0.25\ atm)}$	0.198	0.203	0.209	0.214	0.219
$A_{H2O\ (0.25\ atm)}$	0.126	0.128	0.130	0.132	0.134

The expected absorbance increases are observed for both CO and H_2O, although the increase is proportionally greater for CO (11%) than H_2O (6%). This may be due to a higher density of saturated transitions within the filter envelope for CO. Different air broadening parameters for CO and H_2O [12] may also have a small effect. The increases are sufficiently large to merit a post-measurement correction to meet PMR control requirements.

4.0 CONCLUSIONS

The primary goal of this work is to determine the suitability of the Infraran sensor for use in the Palladium Membrane Reactor. This application presents a challenge for the sensor, since the process temperature exceeds its designed operating range. We have demonstrated that large baseline offsets, comparable to the sensor response to the analyte, are obtained if cool air is blown across the sensor. We have also shown that there is a strong environmental component to the noise. However, the current arrangement does not utilize a reference detector. The strong correlation between the CO and H_2O sensor responses to environmental changes indicate that a reference detector can greatly reduce the environmental sensitivity. In fact, incorporation of a reference detector is essential for the sensor to work in this application.

We have also shown that the two sensor responses are adequately independent. Still, there are several small corrections which must to be made to the sensor response to accommodate chemical and physical effects. Interactions between the two analytes will alter the relationship between number density and pressure. Temperature and pressure broadening will alter the relationship between absorbance and number density. The individual effects are small – on the order of a few percent or less – but cumulatively significant. Still, corrections may be made if temperature and total pressure are independently measured and incorporated into a post-analysis routine. Such corrections are easily programmed and automated and do not represent a significant burden for installation.

---

[*] HITRAN does not provide any means for distinguishing pressure broadening effects due to different gases, e.g. the broadening of CO from water instead of air. Further literature searching or empirical measurements may be required to determine precisely any required correction.

The measurements and simulations described above indicate that with appropriate corrections, the Infraran sensor can approach the 1-1.5% measurement accuracy required for effective PMR process control.

It is also worth noting that the Infraran may be suitable for other gas sensing applications, especially those that do not need to be made in a high-temperature environment. Any gas with an infrared absorption (methane, ammonia, etc.) may be detected so long as an appropriate bandpass filter can be manufactured. Note that homonuclear diatomic molecules (hydrogen and its isotopes, nitrogen, oxygen) do not have infrared absorptions. We have shown that the sensor response may be adequately predicted using commercially available software. Measurement of trace concentrations is limited by the broad spectral bandpass, since the total signal includes non-absorbed frequencies. However, cells with longer pathlengths can be designed to address this problem.

5.0 ACKNOWLEDGEMENTS

We would like to thank H.T. Sessions of SRNL for assistance with incorporation of the sensor into the PMR manifold.

6.0 REFERENCES

[1]   R.S. Willms and K. Okuno, "Recovery of hydrogen from impurities using a palladium membrane reactor", Proc. 15th IEEE Symp. On Fusion Eng., Hyannis, MA, Oct. 11-15, 1993, 85-90.

[2]   S.A. Birdsell, R.S. Willms, P. Arzu, and A. Costello, "Effect of inlet conditions on the performance of a palladium membrane reactor", Proc. 17th IEEE/NPS Symp. On Fusion Eng., San Diego, CA, Oct 6-10, 1997, 301-303.

[3]   S.A. Birdsell and R.S. Willms, "Tritium recovery from tritiated water with a two-stage palladium membrane reactor", *Fusion Eng. and Design* **39-40** (1998) 1041-1048.

[4]   K.D. Cleaver, "The analysis of process gases: a review", *Accred. Qual. Assur.* **6** (2001) 8-15.

[5]   P.T. Jaakkola *et al.*, "On-line analysis of stack gas composition by a low resolution FT-IR gas analyzer", *Water, Air, and Soil Pollution* **101** (1998) 79-92.

[6]   J. Bak and S. Clausen, "FTIR emission spectroscopy methods and procedures for real time quantitative gas analysis in industrial environments", *Meas. Sci. Technol.* **13** (2002) 150-156.

[7]   I. Linnerud, P. Laspersen, and T. Jaeger, "Gas monitoring in the process industry using diode laser spectroscopy", *Appl. Phys. B* **67** (1998) 297-305.

[8]   G. Berden, R. Peeters, and G. Meijer, "Cavity ring-down spectroscopy: Experimental schemes and applications", *Int. Rev. Phys. Chem.* **19** (2000) 565-607.

[9]   P.A. Wilks, "In-line infrared sensors covering the mid-infrared from 2 to 14 μm (5000 to 700 cm^{-1})", *Proc. SPIE* **4577** (2002) 76-82.

[10] W. McKinney, Black Body Emission Calculator, http://infrared.als.lbl.gov/calculators/bb2001.html, 2001.

[11] David R. Lide, ed., *CRC Handbook of Chemistry and Physics, Internet Version 2005,* <http://www.hbcpnetbase.com>, CRC Press, Boca Raton, FL, 2005.

[12] L.S. Rothman *et al.*, "The HITRAN molecular spectroscopic database: edition of 2000 including updates through 2001", J. Quant. Spectrosc. Rad. Transfer **82** (2003) 5-44.

[13] W. Demtröder, *Laser Spectroscopy*, 3rd printing, Springer-Verlag, Berlin, 1988.